Biogeosciences

Open Access

EGU

Equatorward phytoplankton migration during a cold spell within the Late Cretaceous super-greenhouse

Niels A. G. M. van Helmond[1], Appy Sluijs[1], Nina M. Papadomanolaki[1], A. Guy Plint[2], Darren R. Gröcke[3], Martin A. Pearce[4], James S. Eldrett[5], João Trabucho-Alexandre[3,6], Ireneusz Walaszczyk[7], Bas van de Schootbrugge[1], and Henk Brinkhuis[1,8]

[1]Marine Palynology and Paleoceanography, Laboratory of Palaeobotany and Palynology, Department of Earth Sciences, Faculty of Geosciences, Utrecht University, Heidelberglaan 2, 3584 CS Utrecht, the Netherlands
[2]Department of Earth Sciences, The University of Western Ontario, London, Ontario N6A 5B7, Canada
[3]Department of Earth Sciences, Durham University, South Road, Durham DH1 3LE, UK
[4]Evolution Applied Ltd, 50 Mitchell Way, Upper Rissington, Cheltenham, Gloucestershire GL54 2PL, UK
[5]Shell International Exploration and Production Inc., Kesslerpark 1, 2288 GS Rijswijk, the Netherlands
[6]Comparative Sedimentology Group, Department of Earth Sciences, Faculty of Geosciences, Utrecht University, Heidelberglaan 2, 3584 CS Utrecht, the Netherlands
[7]Institute of Geology, Faculty of Geology, University of Warsaw, Zwirki I Wigury 93, 02-089 Warsaw, Poland
[8]NIOZ, Royal Netherlands Institute for Sea Research, P.O. Box 59, 1790 AB Den Burg, Texel, the Netherlands

*Correspondence to:* Niels A. G. M. van Helmond (n.vanhelmond@uu.nl)

Abstract. Oceanic Anoxic Event 2 (OAE2), a ~ 600 kyr episode close to the Cenomanian–Turonian boundary (ca. 94 Ma), is characterized by relatively widespread marine anoxia and ranks amongst the warmest intervals of the Phanerozoic. The early stages of OAE2 are, however, marked by an episode of widespread transient cooling and bottom water oxygenation: the Plenus Cold Event. This cold spell has been linked to a decline in atmospheric $p\text{CO}_2$, resulting from enhanced global organic carbon burial. To investigate the response of phytoplankton to this marked and rapid climate shift we examined the biogeographical response of dinoflagellates to the Plenus Cold Event. Our study is based on a newly generated geochemical and palynological data set from a high-latitude Northern Hemisphere site, Pratts Landing (western Alberta, Canada). We combine these data with a semi-quantitative global compilation of the stratigraphic distribution of dinoflagellate cyst taxa. The data show that dinoflagellate cysts grouped in the *Cyclonephelium compactum–membraniphorum* morphological plexus migrated from high to mid-latitudes during the Plenus Cold Event, making it the sole widely found (micro)fossil to mark this cold spell. In addition to earlier reports from regional metazoan migrations during the Plenus Cold Event, our findings illustrate the effect of rapid climate change on the global biogeographical dispersion of phytoplankton.

1 Introduction

The Cenomanian–Turonian boundary interval (ca. 94 Ma) was an episode of extreme warmth, with tropical and mid-latitude sea surface temperatures exceeding 35 °C (e.g., Huber et al., 2002; Forster et al., 2007; Van Helmond et al., 2014a). This interval corresponds to Oceanic Anoxic Event 2 (OAE2), during which an increase in the production of organic carbon and a reduction in the oxygen content of seawater resulted in unusually high organic matter content of marine sediments (e.g., Schlanger and Jenkyns, 1976; Jenkyns, 2010). The OAE2 interval is stratigraphically marked by a positive carbon isotope excursion in all active carbon reservoirs, resulting from elevated organic carbon burial rates (e.g., Tsikos et al., 2004).

The early stages of OAE2 are characterized by a short-lived (ca. 40 kyr; Jarvis et al., 2011) colder interval as
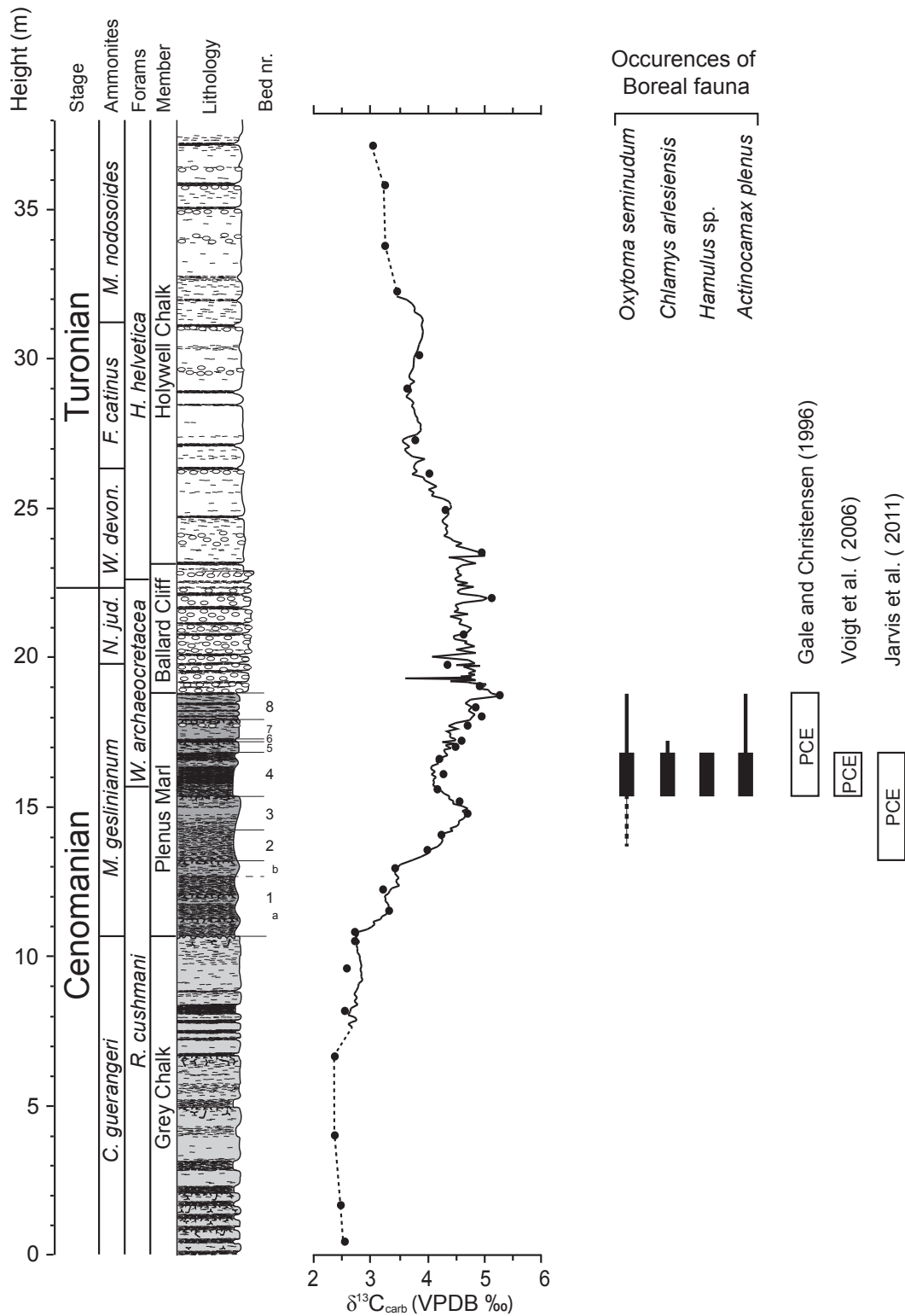
Figure 1. Biozonation, lithology, Plenus Marl beds (Jefferies, 1963) and $\delta^{13}C_{carb}$ (low-resolution data (dots and dotted line) derived from Pearce et al., 2009; high-resolution data (solid line) derived from Paul et al., 1999) for the Cenomanian–Turonian boundary reference section at Eastbourne, combined with occurrences of Boreal fauna (Gale and Christensen, 1996). On the right side the ranges of the different definitions for the Plenus Cold Event are indicated.

recorded in several marine paleotemperature records (e.g., Gale and Christensen, 1996; Forster et al., 2007; Sinninghe Damsté et al., 2010). It was first recognized as the co-occurrence of Boreal fauna with a positive oxygen isotope excursion of about 1.5‰, recorded in biogenic calcite from beds 4–8 of the Plenus Marl in mid-latitude shelf sites of northwestern Europe (Gale and Christensen, 1996). This interval was termed the "Plenus Cold Event" (PCE; Fig. 1), after the Boreal belemnite *Praeactinocamax plenus* (Blainville). Subsequently, the PCE was restricted only to Bed 4 of the Plenus Marl, being the sole bed containing abundant Boreal fauna (Voigt et al., 2006; Fig. 1). Bed 4 corresponds precisely to the upper trough and second build-up of the carbon isotope excursion, the upper part of the *Metoicoceras geslinianum* ammonite zone and basal *Whiteinella archaeocretacea* planktonic foraminifer zone (Gale et al., 2005). More recently, Jarvis et al. (2011) extended the PCE down to beds 2 and 3 of the Plenus Marl (Fig. 1), based on a positive excursion in carbonate oxygen isotopes.

The PCE interval is characterized by a 3–7 °C cooling of sea surface temperatures in the proto-North Atlantic and the European shelf (e.g., Forster et al., 2007; Sinninghe Damsté et al., 2010; van Helmond et al., 2014a, 2015). In several regions, such as the Western Interior Seaway (Eldrett et al., 2014) and proto-North Atlantic (e.g., Forster et al., 2007), the stratigraphic position of the PCE is characterized by minima in sediment organic carbon content and redox-sensitive element concentrations, which indicates improved oxygenation of bottom waters (e.g., van Helmond et al., 2014b). Furthermore the stratigraphic position of the PCE coincides with a decline in atmospheric $p\mathrm{CO_2}$ (e.g., Kuypers et al., 1999; Sinninghe Damsté et al., 2008; Barclay et al., 2010), which is thought to be a consequence of enhanced sequestration of organic carbon in sediments during the early stages of OAE2 (e.g., Barclay et al., 2010; Sinninghe Damsté et al., 2010). The incursion of Boreal fauna into lower latitudes has only been documented for the European shelf. A causal relation between $p\mathrm{CO_2}$ drawdown, sea surface cooling, bottom water oxygenation and the PCE has been proposed (e.g., Forster et al., 2007; Sinninghe Damsté et al., 2010; Jarvis et al., 2011; van Helmond et al., 2014b).

Previously, it remained unclear as to whether the migration of Boreal fauna was related to a migration of multiple components of marine food webs. Recently, van Helmond et al. (2014a, 2015) showed that the first consistent presence (FCP; presence of multiple specimens in consecutive samples) of dinoflagellate cysts (dinocysts) belonging to the *Cyclonephelium compactum–membraniphorum* morphological plexus (*Ccm*; see below for a detailed discussion on taxonomic status) in two sections on the proto-North Atlantic and European shelf coincided with a cooling of sea surface temperatures at the stratigraphic level of the PCE. To test whether *Ccm* was truly a high-latitude taxon and whether widespread migration of these dinoflagellates occurred during the PCE, we studied a high-latitude site in northwestern

Alberta, Canada (Pratts Landing), and compiled a global distribution of *Ccm* across OAE2, calibrated using biostratigraphy and carbon isotope stratigraphy.

2 Materials and methods

2.1 Stratigraphic setting of the Pratts Landing section

In northwestern Alberta and northeastern British Columbia, upper Cenomanian and Turonian strata of the Kaskapau Formation form a thick, mudstone-dominated and northeastward-thinning wedge that spans the foredeep of the Western Canada Foreland Basin (Varban and Plint, 2005). Well-exposed sections in the Rocky Mountain Foothills on the western margin of the foredeep can be correlated with sections in the Peace River Valley, located close to the forebulge. Correlation has been established by using abundant, publicly accessible wireline log data (Fig. 2). Detailed correlation through a grid of 756 wireline logs showed that 28 allomembers, bounded by marine flooding surfaces, could be mapped across the foredeep (Varban and Plint, 2005). In the western part of the foredeep, exemplified by the section at Mount Robert (Figs. 2, 3), nearshore and shoreface sandstones form stacked successions that prograded only 20–40 km seaward from the preserved basin margin; shoreface progradation was limited by a consistently high rate of flexural subsidence (Varban and Plint, 2005, 2008). Traced eastward from Mount Robert, successive allomembers become thinner and finer-grained, and some allomembers (e.g., allomembers 7, 9, 10) pinch out completely before reaching outcrop in the Peace River Valley, exemplified by the section at Pratts Landing (Figs. 2, 3). The section at Pratts Landing, which is the focus of this study, is located on the northern bank of the Peace River (56°01′14″ N, 118°48′47″ W; Fig. 4) and comprises stacked siltier- and sandier-upward successions, capped, at a prominent flooding surface, by weakly bioturbated, organic-rich claystones and silty claystones characterized by a very high radioactivity (i.e., boundary of allomembers 6 and 8; Figs. 3, 5). Outcrop spectral gamma ray profiles allow the Pratts Landing section to be correlated with confidence to nearby wireline logs (Fig. 3).

In the west, the Cenomanian–Turonian boundary was recognized at the top of Kaskapau allomember 6 at Mount Robert, based on the distribution of inoceramid bivalves (Fig. 3). At that section, late Cenomanian *Inoceramus* ex gr. *pictus* (Sowerby) is widely distributed through allomembers 2 to 6, whereas *Mytiloides puebloensis* (Walaszczyk and Cobban) is present 2 m above the allomember 6–7 contact, indicating that the lowest zone of the Turonian is present in the lower part of allomember 7 (cf. Kennedy et al., 2000). The upper bounding surface of allomember 6 can be traced, through well logs, for 220 km eastward to Pratts Landing, where it corresponds to the sharp basal surface of a gypsum-cemented silty claystone. That sharp surface, separating al-
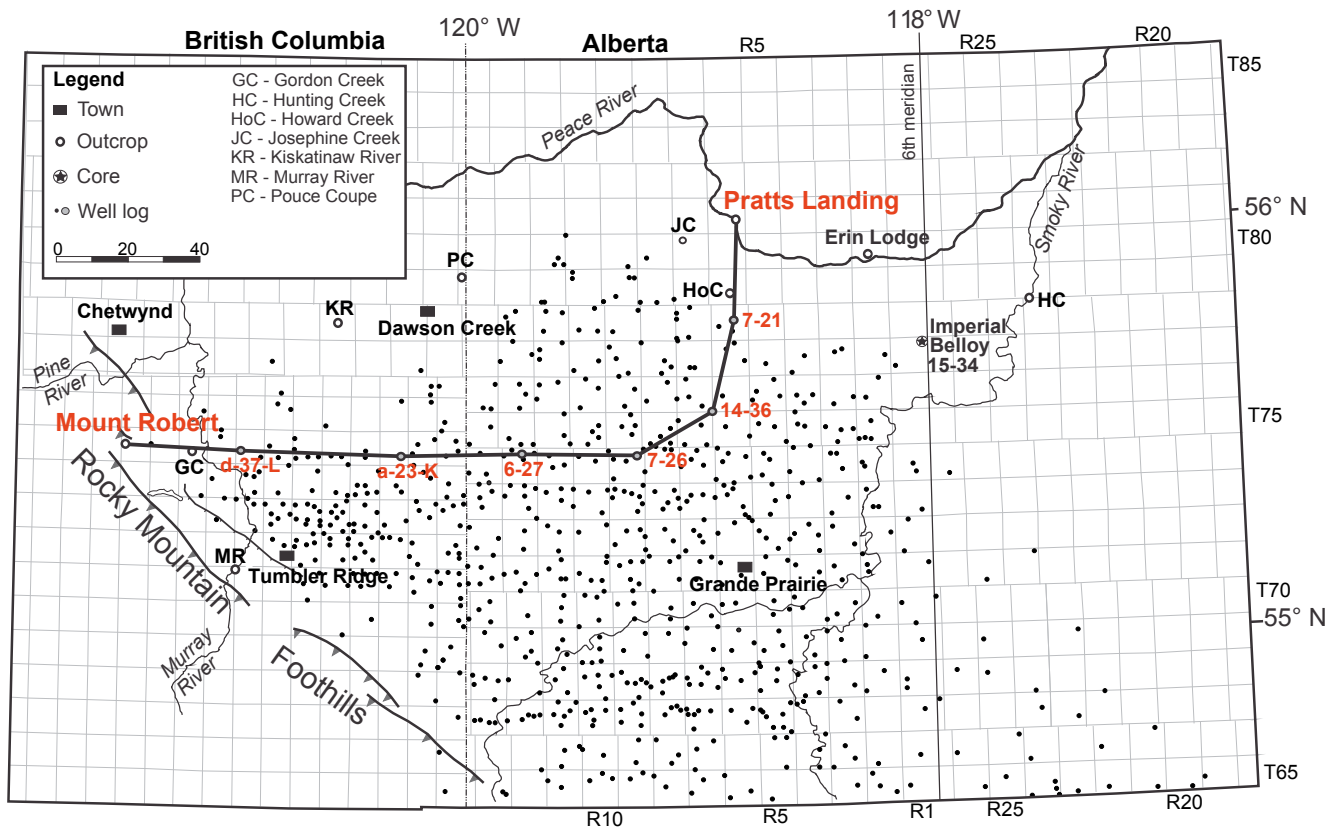
Figure 2. Map of northwestern Alberta and adjacent British Columbia showing distribution of well logs, cores and outcrops used to establish the regional stratigraphic framework that forms the basis for the present study. Outcrop sections at Mount Robert in the west and Pratts Landing in the east are correlated via wireline well logs (gamma ray and resistivity pairs).

lomembers 6 and 8, corresponds to an abrupt increase in radioactivity, and lies 25 cm below the first appearance of the early Turonian inoceramids *Mytiloides goppelnensis* (Badillet and Sornay) and *Mytiloides kossmati* (Heinz; Figs. 3, 5). The wireline log correlation shows that, at Pratts Landing, all of allomember 7 is missing, and the earliest Turonian zone of *M. puebloensis* also appears to be unrepresented, emphasizing the hiatal character of the allomember 6–8 boundary (Fig. 3).

During the Late Cretaceous, the study site was located at $\sim \pm 5\,61°$ N (van Hinsbergen et al., 2015; paleolatitude.org), on the eastern flank of the foredeep, about 160 km from the contemporaneous western shoreline of the Western Interior Seaway (Varban and Plint, 2005, 2008). We generated carbon isotope and dinoflagellate cyst data across about 23 m of upper Cenomanian to lower Turonian strata, based on stable carbon isotope stratigraphy and inoceramid biostratigraphy (Figs. 3, 6).

2.2 Stable isotope geochemistry

The carbon isotope composition of bulk organic carbon ($\delta^{13}C_{org}$) was measured at 20 cm intervals across OAE2 in

order to constrain its exact position, and at 50 cm intervals for the remainder of the section. Analyses were performed in the Stable-Isotope Biogeochemistry Laboratory of the School of Geography and Earth Sciences, McMaster University, Hamilton, Ontario, Canada. In total, 77 samples were treated with 3 N HCl to remove carbonates, rinsed with demineralized water, freeze-dried and powdered. Between 1 and 3 mg of powdered sediment sample was weighed in tin capsules and then put in a rotating carousel for subsequent combustion in an elemental analyzer. After purification of the gas sample it was passed through a SIRA II Series 2 dual-inlet isotope-ratio mass spectrometer to determine the stable carbon isotopic composition of organic matter. Carbon isotope ratios were measured against an international standard, NBS-21. The analytical reproducibility, based on replicate samples, was better than 0.1 ‰.

2.3 Palynological processing

Dinocyst abundances were determined for 21 samples, covering the entire section, using standard palynological methods. About 5 g of freeze-dried sediment was processed following a standardized quantitative method (e.g., Sluijs et al.,
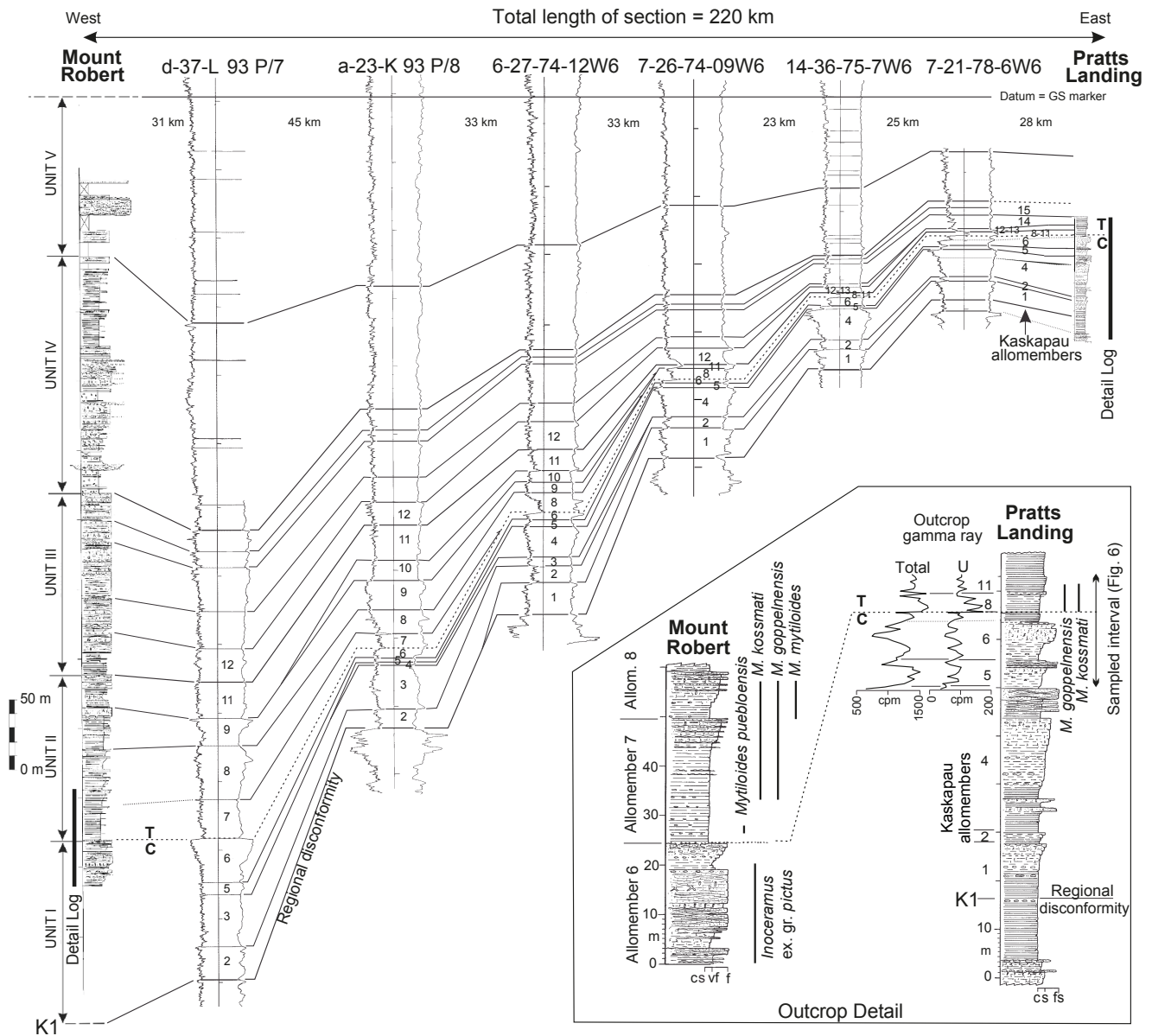
Figure 3. Regional cross section (located in Fig. 2) showing how allomembers of the Kaskapau Formation can be correlated across the foredeep from Mount Robert to Pratts Landing. Cross section is condensed from more detailed lines in Varban and Plint (2005). The Cenomanian–Turonian boundary is shown as a broken line at the top of allomember 6. Note how allomember 7 laps out eastward onto allomember 6, and that both allomembers 6 and 8 become increasingly radioactive towards the east. Spectral gamma ray profiles taken at Pratts Landing confirm the correlation of the various stratal units at outcrop with their equivalents in subsurface. The inset stratigraphic logs show more detailed representations of the lithological successions, gamma ray profiles, and the distribution of inoceramid bivalves at Mount Robert and Pratts Landing. Detailed legend in Fig. 6.

2003), which involves the addition of a known amount of *Lycopodium* marker spores (Stockmar, 1971). To dissolve carbonates and silicates, HCl ($\sim 30\%$) and HF ($\sim 38\%$) were added, respectively. After centrifugation, acids were discarded. The remaining residues were sieved over a 15 μm nylon mesh and the > 15 μm fraction was mounted on slides for analysis by light microscopy. Samples were counted to a minimum of 250 dinocysts, which were identified to genus
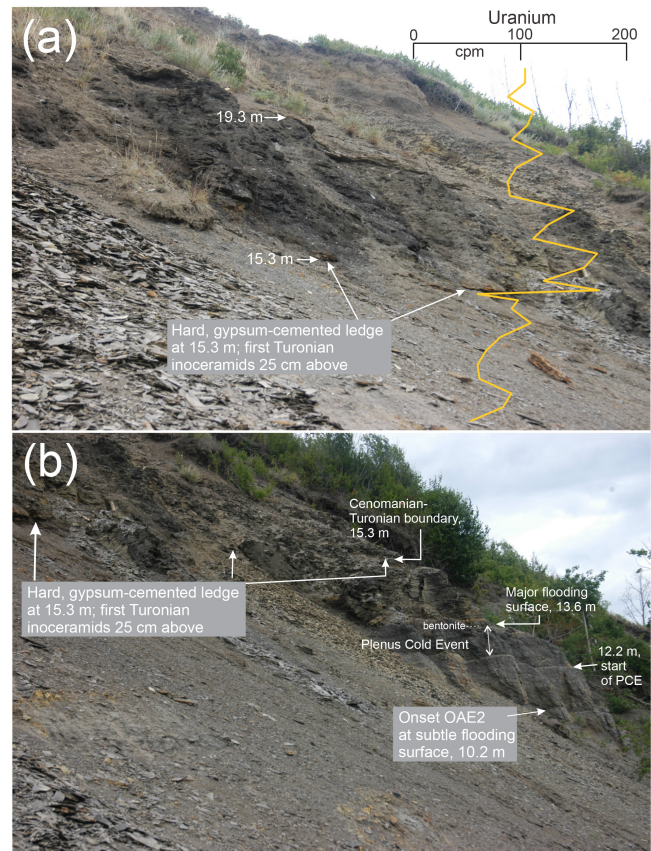
or species level at $500\times$ magnification, following the taxonomy of Fensome and Williams (2004). All samples and slides are stored in the collection of the Laboratory of Palaeobotany and Palynology, Utrecht University, the Netherlands. All data ($\delta^{13}C_{org}$ and palynology) are listed in the Supplement (Table S1).
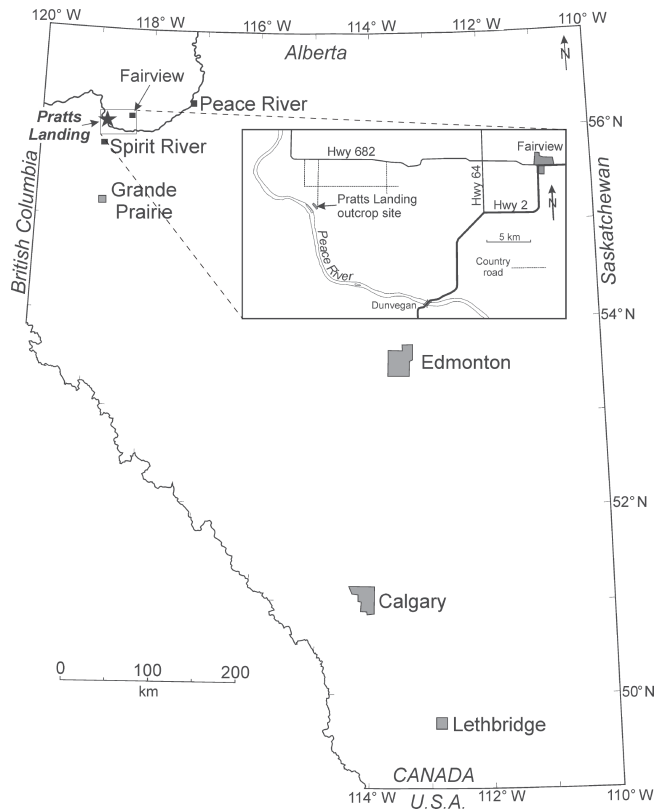
Figure 4. Map showing the southern part of Alberta. The study site at Pratts Landing is located on the Peace River about 70 km east of the Alberta–British Columbia border. Inset map shows details of the Peace River area in the vicinity of the town of Fairview, with the outcrop locality and access roads indicated.

Figure 5. Field photographs of the Pratts Landing site. Photograph **(a)** shows an overview of upper part of the section showing resistant, gypsum-cemented ledge that marks a sharp erosional boundary between two claystone units. Immediately above the boundary there is a large increase in the uranium content of the sediment. The early Turonian inoceramid bivalves *Mytiloides goppelnensis* and *Mytiloides kossmati* appear 25 cm above the erosion surface. Photograph **(b)** shows an overview of the lower part of the section showing highly bioturbated silty sandstone of Kaskapau allomember 6, sharply overlain, at a major flooding surface (13.6 m level in Fig. 6) by thinly bedded claystones. Rocks embracing the Plenus Cold Event are represented by a 1.4 m thick, shallowing (sandier)-upward succession bounded above by a major flooding surface. The Cenomanian–Turonian boundary, marked by a resistant ledge, lies at the 15.3 m level. Note that all of Kaskapau allomember 7 is absent at the erosion surface marking the Cenomanian–Turonian boundary, as illustrated in Fig. 3.

2.4 Taxonomy and literature survey

Originally the cysts *Cyclonephelium membraniphorum* (Cookson and Eisenack, 1962), which was renamed *Cauveridinium membraniphorum* (Masure in Fauconnier and Masure, 2004), were differentiated from *Cyclonephelium compactum* (Deflandre and Cookson, 1955), based on the generally higher and structurally ordered crests and membranes of *C. membraniphorum*. Additionally, cysts of *C. membraniphorum* form a series of funnel-shaped structures bordering unornamented mid-dorsal and mid-ventral areas. However, the apparent morphological variation regarding ornamentation within the two species exceeds the defined difference between the two species. Therefore, it was proposed to refer to the dinocyst morphological complex *Cyclonephelium compactum–membraniphorum*, rather than separating both species (Marshall and Batten, 1988). We agree that the two species are members of a morphological continuum and therefore group all these morphotypes of this continuum from our study site and the literature under the *Cyclonephelium compactum–membraniphorum* morphological plexus (*Ccm*) (Fig. 7; Table 1). For the compilation of the

global biogeographical distribution of *Ccm* prior to, during and after OAE2, a literature survey was conducted.

3 Results and discussion

3.1 Dinocyst biogeography

At Pratts Landing the OAE2 interval is recorded between 10.2 and 16.8 m, based on a 2 ‰ positive shift in $\delta^{13}C_{org}$

Table 1. Overview of the localities where cysts of *Cyclonephelium compactum–membraniphorum* morphological plexus (*Ccm*) have been reported across the Cenomanian–Turonian boundary interval. In the fourth and fifth column an "X" marks whether the first consistent presence (FCP) of *Ccm* was before OAE2 or whether it was associated with the first maximum in the positive carbon isotopic excursion (CIE), point "A" (cf. Voigt et al., 2008). Question marks indicate that the FCP could not be determined accurately, resulting from insufficient supporting information, e.g., high-resolution carbon isotope stratigraphy or unquantified abundances of *Ccm*. Localities further discussed in the article are in bold. WIS: Western Interior Seaway.

Site ID	Region	Locality	FCP of *Ccm* prior to OAE2	FCP of *Ccm* associated with CIE-"A"	References
North America					
1	WIS	Blue Point, Arizona, USA		X	Li and Habib (1996), Harris and Tocher (2003)
a	**WIS**	**Shell Iona-1, Texas, USA**		X	**Eldrett et al. (2014)**
2	WIS	Pueblo, Colorado, USA		X	Dodsworth (2000), Harris and Tocher (2003)
3	WIS	Wahweap Wash, Utah, USA		?	Harris and Tocher (2003)
4	WIS	Bunker Hill, Kansas, USA		?	Harris and Tocher (2003)
5	WIS	Rebecca K. Bounds Core, Kansas, USA		?	Harris and Tocher (2003)
b	**WIS**	**Pratts Landing, Alberta, Canada**	X		**this study**
c	**proto-N. Atlantic shelf**	**Bass River, New Jersey, USA**		X	**van Helmond et al. (2014a)**
Europe					
6	European shelf	Lulworth, Dorset, UK		X	Dodsworth (2000)
7	European shelf	Culver Cliff, Isle of Wight, UK		X	Lignum (2009)
8	European shelf	Folkstone, Kent, UK		X	Jarvis et al. (1988), Lignum (2009)
d	**European shelf**	**Eastbourne, East Sussex, UK**		X	**Pearce et al. (2009)**
9	European shelf	Eastern UK	?	?	Dodsworth (1996)
e	**European shelf**	**Wunstorf, Lower Saxony, Germany**		X	**Marshall and Batten (1988), Prauss (2006), Lignum (2009), van Helmond et al. (2015)**
10	European shelf	Misburg, Lower Saxony, Germany		X	Marshall and Batten (1988)
11	European shelf	Norwegian Sea, Norway	X		Radmacher et al. (2015)
12	European shelf	Gröbern, Saxony Anhalt, Germany		X	Lignum (2009)
13	European shelf	Ratssteinbruch, Saxony, Germany		X	Lignum (2009)
14	European shelf	Pulawy, central Poland		X	Dodsworth (2004a)
15	European shelf	Nymburk, Central Bohemia, Czech Republic		?	Čech et al. (2005)
16	European shelf	Aksudere, Crimea		?	Dodsworth (2004b)
17	European shelf	Bois du Gallet, St.-Sylvestre-de-Cormeilles, Normandy, France		?	Tocher and Jarvis (1995)
18	European shelf	Les Fosses Blanches, Duneau, Maine, France		?	Tocher and Jarvis (1995)
19	European shelf	Ganuza, Castilian Platform, Spain		?	Lamolda and Mao (1999)
20	European shelf	Puentedey, Castilian Platform, Spain		?	Peyrot et al. (2011)
21	European shelf	Fuentetoba, Castilian Plateau, Spain		?	Peyrot et al. (2011)
22	European shelf	Tamajon, Castilian Plateau, Spain		?	Peyrot et al. (2011)
23	European shelf	Condemios, Castilian Plateau, Spain		?	Peyrot et al. (2012)
24	Tethys	Ultrahelvetic Rehkogelgraben, Austria		?	Pavlishina and Wagreich (2012)
25	Tethys	Pont d'Issole, Provence-Alpes-Côte d'Azur, France		X	Lignum (2009)
26	Tethys	Vergons, Provence-Alpes-Côte d'Azur, France		X	Courtinat et al. (1991), Lignum (2009)
Southern Hemisphere					
27	Southern Ocean	Central Kerguelen Plateau	?	?	Mohr et al. (2002)
28	Indian Ocean	Northwestern Australia	X		McMinn (1988)
29	Pacific Ocean	East Coast Basin, New Zealand	X		Hasegawa et al. (2013), Schiøler and Crampton (2014)
30	Pacific Ocean	Mangaotane Stream, Raukumara Peninsula, New Zealand	X		Crampton et al. (2001)
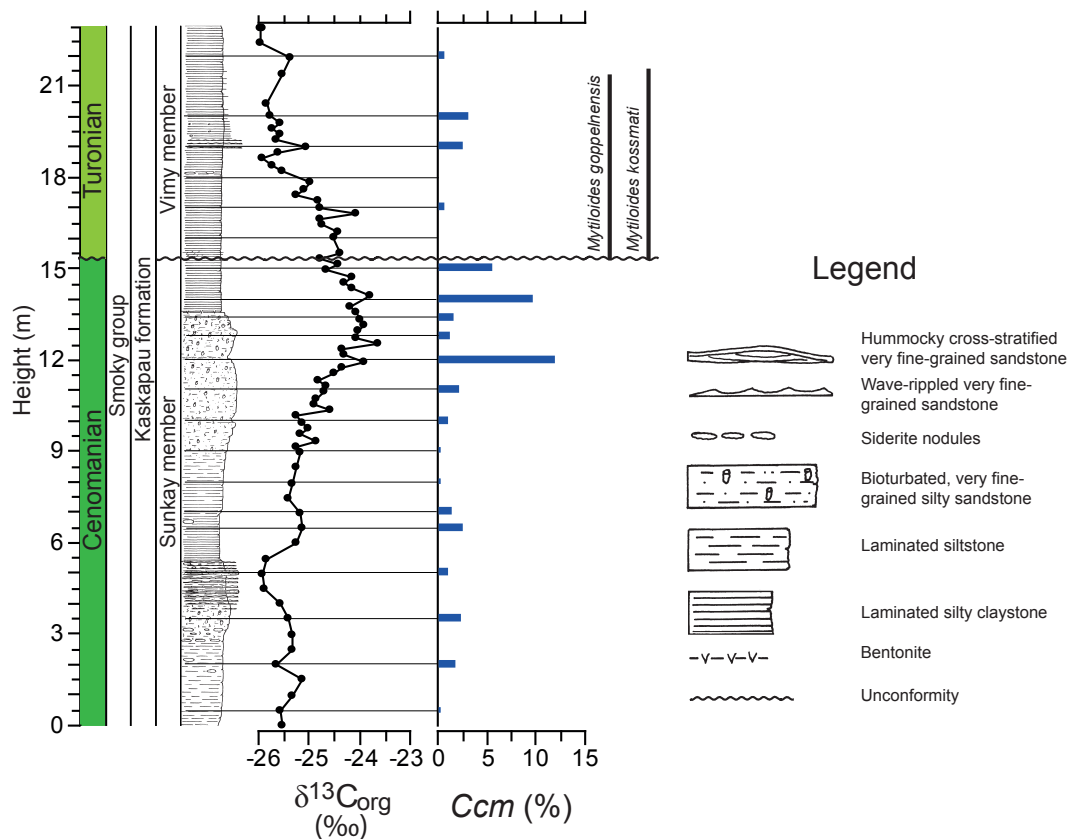
Figure 6. Lithostratigraphy, detailed lithological log, $\delta^{13}C_{org}$, abundances of *Cyclonephelium compactum–membraniphorum* morphological plexus (*Ccm*) and inoceramid bivalve stratigraphy for Pratts Landing. Sample intervals for palynology are indicated by horizontal black lines.

(Fig. 6). The Cenomanian–Turonian boundary is placed at 15.3 m, at the sharp base of a 20 cm thick, heavily gypsum-cemented silty claystone lacking macrofauna (Fig. 5). The base Turonian marker inoceramid species *Mytiloides puebloensis* was not found, but the succeeding inoceramid zone, characterized by *M. goppelnensis* and *M. kossmati*, starts approximately 25 cm above the basal surface (Fig. 3). *Ccm* is a general constituent (1–4 %) of the dinocyst assemblage at Pratts Landing throughout the section, i.e., also below the onset of OAE2 (Fig. 6).

All localities ($n = 35$) with reported cysts of *Ccm* (i.e., *Cauveridinium membraniphorum*, *Cyclonephelium membraniphorum*, *Cyclonephelium compactum* and/or *Cyclonephelium compactum–membraniphorum*) are listed in Table 1 and shown in Fig. 8. The first common presence (FCP) of *Ccm* could only be determined for 20 of the localities as a result of poor stratigraphic constraints and only qualitative reporting of *Ccm* at the other 15 localities.

Recent dinocyst biostratigraphic studies from the East Coast Basin, New Zealand, show that the FCP of *Ccm* was ca. 500 kyr before the onset of OAE2 (Schiøler and Crampton, 2014). At northern high latitudes, notably Pratts Landing and the Norwegian Sea (Radmacher et al., 2015), *Ccm* is a

consistent constituent of the dinocyst assemblage throughout the late Cenomanian. In contrast, at most Northern Hemisphere mid-latitude sites, *Ccm* has not been reported before OAE2, with the exception of a few spot occurrences at Eastbourne and Iona-1 (Pearce et al., 2009; Eldrett et al., 2014). Crucially, *Ccm* was never a consistent constituent of mid-latitude dinocyst assemblages before OAE2. This indicates that *Ccm* had a high-latitude biogeographical distribution in both hemispheres before OAE2.

Five Northern Hemisphere shelf sites in Europe and North America, namely Pratts Landing, Iona-1 (southwestern Texas, USA), Bass River (New Jersey, USA), Eastbourne (East Sussex, UK) and Wunstorf (Lower Saxony, Germany), were selected to compare established biozonation, high-resolution records of $\delta^{13}C$, and the relative abundances of *Ccm* (Fig. 9; Pearce et al., 2009; Eldrett et al., 2014; van Helmond et al., 2014a, 2015). Maximum relative abundances of *Ccm* (i.e., > 10 %) are recorded during the first maximum in the OAE2 characterizing carbon isotope excursion (point "A" – cf. Voigt et al., 2008), at Pratts Landing (Figs. 6, 9). At the same stratigraphic position, *Ccm* becomes abundant at several other Northern Hemisphere mid-latitude sites, for example the southern part of the Western Interior
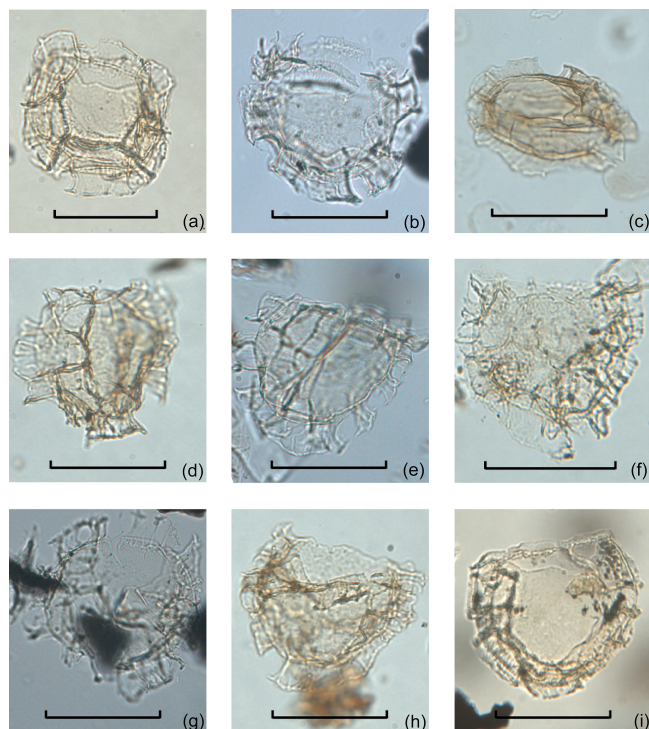
Figure 7. Various specimens of the *Cyclonephelium compactum–membraniphorum* morphological plexus (*Ccm*), gradually changing from the *C. membraniphorum* end-member **(a–c)** to the *C. compactum* end-member **(g–i)**. Specimens **(a)** (England Finder coordinates (EFc): U59/2-slide 1) and **(i)** (EFc: L70/1-slide 2) are from Wunstorf sample 42.21 m.b.s. (meters below surface), specimen **(b)** (EFc: H13-slide 1) is from Bass River sample 590.69 m.b.s, specimen **(c)** (EFc: R65/1-slide 1) is from Wunstorf sample 45.81 m.b.s, specimens **(d)** (EFc: M59/2-slide 1) and **(h)** (EFc: V53/2-slide 1) are from Pratts Landing sample 6.5 m, specimens **(e)** (EFc: E59/2-slide 1) and **(g)** (EFc: T64/3-slide 2) are from Bass River sample 590.08 m.b.s, and specimen **(f)** (EFc: J8/1-slide 1) is from Pratts Landing sample 12 m. Scale bars represent 50 µm.

Seaway, the proto-North Atlantic shelf, the European shelf, and the Tethys (Figs. 8, 9; Table 1). Despite a spot occurrence at point "A", the FCP of *Ccm* seems somewhat delayed at Eastbourne (i.e., Plenus Marl Bed 7 – Fig. 9; Pearce et al., 2009); this is a local phenomenon, because in other English Chalk sections (e.g., Dodsworth, 2000) the FCP of *Ccm* coincides with that of other Northern Hemisphere mid-latitude sites.

3.2 Ecology

At Bass River and Wunstorf the FCP of *Ccm* precisely correlates with a drop in sea surface temperature (van Helmond et al., 2014a, 2015), leading to the suggestion that the dinoflagellate taxon that produced *Ccm* migrated to these sites in response to climatic cooling. We therefore suggest that sea surface temperature was the primary control on the biogeo-

graphical distribution of *Ccm* outside high-latitude regions. For the Shell Iona-1 core the FCP of *Ccm* coincides with a minimum in organic carbon, redox-sensitive elements and relatively high abundances of benthic foraminifera and trace fossils indicative of a period of improved oxygenation of bottom waters (Eldrett et al., 2014). This is in agreement with previous observations for the interval showing PCE-related cooling of sea surface temperature in the proto-North Atlantic (Forster et al., 2007; Sinninghe Damsté et al., 2010; van Helmond et al., 2014b). The sustained presence of *Ccm* after the PCE at all sites, except Bass River (Fig. 9), suggests that, in addition to sea surface temperature, other environmental and paleoceanographic factors became dominant in determining the distribution of *Ccm* once it had occupied niches at lower latitudes. For example, salinity, (enhanced) nutrient availability and proximity to the shoreline may have been important (Harris and Tocher, 2003). Preservation of palynomorphs, e.g., dinocysts, is variable within sections and between sections but is unrelated to the occurrences of certain species.

The migration of *Ccm* towards lower latitudes in response to cooling resembles dinoflagellate migration events during other periods of marked climatic change. Dinocysts referable to the Arctic Paleogene taxon *Svalbardella* were encountered in mid- and low latitudes during the most pronounced Oligocene glaciations (ca. 30–25 Ma; van Simaeys et al., 2005). In contrast, during the Paleocene–Eocene Thermal Maximum, tropical species of the dinocyst genus *Apectodinium* moved from low toward high latitudes in response to peak warmth (Crouch et al., 2003; Sluijs et al., 2007). Studies across the Cretaceous–Paleogene boundary indicate initial high latitude to equatorial dinoflagellate migration at the boundary, followed by a reverse migration. This presumably took place in response to impact-related initial climatic cooling followed by a return to warmer conditions (Brinkhuis et al., 1998; Galeotti et al., 2004; Vellekoop et al., 2014).

The biogeographical expansion of *Ccm* towards the Equator seems to be a relatively strong response to a moderate change in sea surface temperature (ca. 3–5 °C). The southward migration of *Ccm* over relatively large distances, i.e., 20–30° of latitude southwards, may have been amplified by the flatter meridional temperature gradients across OAE2 (e.g., Sinninghe Damsté et al., 2010). Compared to the present day, which is characterized by a much steeper meridional temperature gradient, relatively small changes in temperature in the mid-Cretaceous and early Paleogene may have had a much larger impact on the distribution of marine organisms.

3.3 A new stratigraphic marker

Most of the Cretaceous is covered by the Normal Superchron C34n (ca. 126–84 Ma; Gradstein et al., 2012), hampering application of magnetostratigraphy. Stratigraphic correlation for the Cenomanian–Turonian boundary interval there-
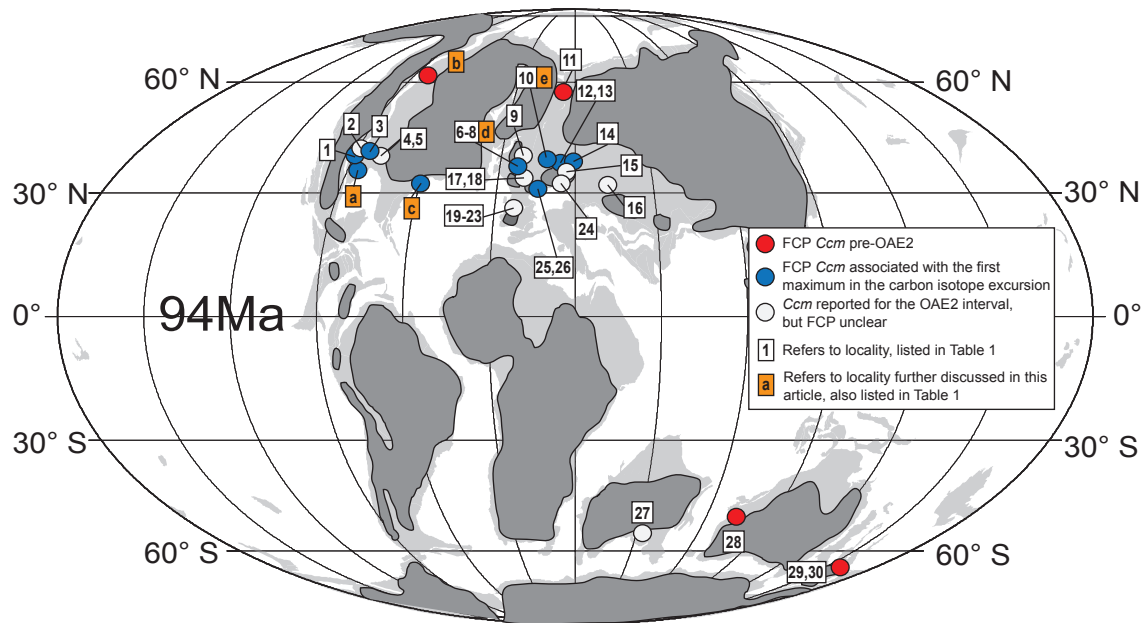
Figure 8. Compilation of the first consistent presence (FCP) of *Cyclonephelium compactum–membraniphorum* morphological plexus (*Ccm*) across Oceanic Anoxic Event 2. Numbers in white boxes refer to localities compiled in Table 1. Letters in orange boxes refer to the sites selected for comparison of established biozonation, high-resolution records of δ^{13}C and the relative abundances of *Ccm* (Fig. 9) also compiled in Table 1. The Mollweide projected paleogeographic map for the Cenomanian–Turonian boundary interval was generated at http://www.odsn.de/odsn/services/paleomap/paleomap.html. Continental plates are in light gray. Dry land in dark gray after Scotese (2001).

fore relies on biostratigraphy and carbon isotope stratigraphy (Gale et al., 2005) as well as on recent advances in astrochronology (e.g., Meyers et al., 2012; Eldrett et al., 2015). Pelagic sediments are often carbonate-poor, because the calcite compensation depth was relatively shallow during OAE2, complicating planktonic foraminifer and calcareous nannofossil biostratigraphy (e.g., Erba, 2004). Consequently, carbon isotope stratigraphy is the main stratigraphic tool for OAE2 because the positive carbon isotope excursion is recognized in all active carbon reservoirs (Tsikos et al., 2004). Calibration of carbon isotope stratigraphy with bioevents is, however, essential to establish detailed stratigraphic frameworks.

The coincidence of the FCP of *Ccm* with the base of the *W. archaeocretacea* and the upper part of the *M. geslinianum* zones close to the first maximum in the positive carbon isotope excursion (point "A"; Fig. 9) suggests that dinoflagellate migration probably occurred within thousands to 10 000 years. The FCP of *Ccm* thus represents a useful biostratigraphic marker, being, to date, the only widely found microfossil to mark the PCE, except at high latitudes.
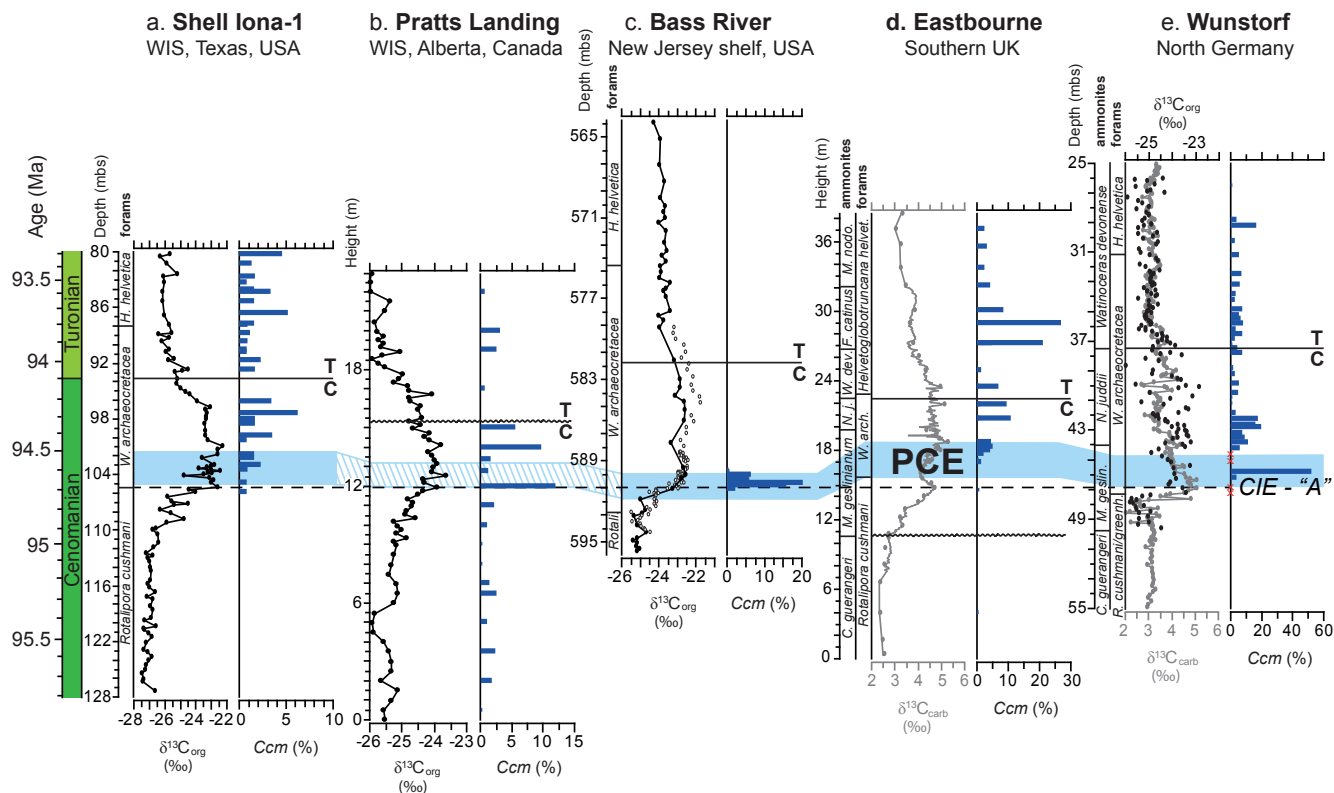
duced the dinocyst morphological complex *Ccm*, from high-latitudes to mid-latitudes during the early stages of OAE2 (latest Cenomanian). The first consistent presence of this taxon at mid-latitudes correlates with the stratigraphic position of the Plenus Cold Event, following its original definition by Gale and Christensen (1996), making it the sole widely distributed microfossil to mark this cold spell. The coincidence of the first consistent presence of *Ccm* in the mid-latitudes with this transient cooling implies lasting reorganization of phytoplankton biogeography in response to rapid climate change during the Late Cretaceous super-greenhouse. The migration of *Ccm* in response to climatic cooling resembles previously recognized dinoflagellate migration events during comparable periods of transient climate change, e.g., the Oligocene glaciations and the Paleocene–Eocene Thermal Maximum.

The Supplement related to this article is available online at doi:10.5194/bg-13-2859-2016-supplement.

4   Conclusions

A global compilation of dinocyst assemblage records combined with new data from a high-latitude site spanning OAE2 illustrates the migration of dinoflagellates, which pro-

Figure 9. Overview of $\delta^{13}C_{org}$ and/or $\delta^{13}C_{carb}$, abundances of *Cyclonephelium compactum–membraniphorum* morphological plexus (*Ccm*) and foraminiferal and/or ammonite zonation for the studied sections. **(a)** Shell Iona-1 core (Eldrett et al., 2014). **(b)** Pratts Landing (this study). **(c)** Bass River (van Helmond et al., 2014a); open symbols are $\delta^{13}C_{org}$ derived from Bowman and Bralower (2005). **(d)** Eastbourne (Pearce et al., 2009); high-resolution $\delta^{13}C_{carb}$ data derived from Paul et al. (1999). **(e)** Wunstorf – relative abundances of *Ccm* from van Helmond et al. (2015), $\delta^{13}C_{org}$ from Du Vivier et al. (2014) and $\delta^{13}C_{carb}$ from Voigt et al. (2008); a red cross marks a barren sample. Age is from the astronomically tuned age model for the Shell Iona-1 core (Eldrett et al., 2015). Dashed line represents the first maximum in the carbon isotope excursion, point "A" (cf. Voigt et al., 2008). Solid lines represent the Cenomanian–Turonian boundary. The blue shaded area represents the Plenus Cold Event according to its original definition (Gale and Christensen, 1996), the cooling in reconstructed sea surface temperatures at Bass River and Wunstorf (van Helmond et al., 2014a, 2015), and the (re)oxygenation of bottom waters in the Shell Iona-1 core (Eldrett et al., 2014). Note: the sections are plotted using different depth scales.

References

Barclay, R. S., McElwain, J. C., and Sageman, B. B.: Carbon sequestration activated by a volcanic CO$_2$ pulse during Oceanic Anoxic Event 2, Nat. Geosci., 3, 205–208, 2010.

Bowman, A. R., and Bralower, T. J.: Paleoceanographic significance of high-resolution carbon isotope records across the Cenomanian–Turonian boundary in the Western Interior and New Jersey coastal plain, USA, Mar. Geol., 217, 305–321, 2005.

Brinkhuis, H., Bujak, J. P., Smit, J., Versteegh, G. J. M., and Visscher, H.: Dinoflagellate-based sea surface temperature reconstructions across the Cretaceous–Tertiary boundary, Palaeogeogr. Palaeocl., 141, 67–83, 1998.

Čech, S., Hradecká, L., Svobodová, M., and Švábenická, L.: Cenomanian and Cenomanian-Turonian boundary in the southern part of the Bohemian Cretaceous Basin, Czech Republic, Bull. Geosci., 80, 321–354, 2005.

Cookson, I. C. and Eisenack, A.: Additional microplankton from Australian Cretaceous sediments, Micropaleontology, 8, 485–507, 1962.

Courtinat, B., Crumière, J. P., Méon, H., and Schaaf, A.: Les associations de kystes de dinoflagellés du Cénomanien-Turonien de Vergons (Bassin Vocontien France), Geobios-Lyon, 24, 649–666, 1991.

Crampton, J. S., Raine, I., Strong, C. P., and Wilson, G. J.: Integrated biostratigraphy of the Raukumara Series stratotype (Cenomanian to Coniacian) at Mangaotane Stream, Raukumara Peninsula, New Zealand, New Zealand, J. Geol. Geop., 44, 365–389, 2001.

Crouch, E. M., Dickens, G. R., Brinkhuis, H., Aubry, M.-P., Hollis, C. J., Rogers, K. M., and Visscher, H.: The *Apectodinium* acme and terrestrial discharge during the Paleocene Eocene thermal maximum: New palynological, geochemical and calcareous nannoplankton observations at Tawanui, New Zealand, Palaeogeogr. Palaeocl., 194, 387–403, 2003.

Deflandre, G. and Cookson, I. C.: Fossil microplankton from Australian late Mesozoic and Tertiary sediments, Mar. Freshwater Res., 6, 242–314, 1955.

Dodsworth, P.: Stratigraphy, microfossils and depositional environments of the lowermost part of the Welton Chalk Formation, late Cenomanian to early Turonian (Cretaceous) in eastern England, P. York. Geol. Soc., 51, 45–64, 1996.

Dodsworth, P.: Trans-Atlantic dinoflagellate cyst stratigraphy across the Cenomanian–Turonian (Cretaceous) Stage boundary, J. Micropalaeontol., 19, 69–84, 2000.

Dodsworth, P.: The distribution of dinoflagellate cysts across a Late Cenomanian carbon isotope (δ^{13}C) anomaly in the Pulawy borehole, central Poland, J. Micropalaeontol., 23, 77–80, 2004a.

Dodsworth, P.: The palynology of the Cenomanian–Turonian (Cretaceous) boundary succession at Aksudere in Crimea, Ukraine, Palynology, 28, 129–141, 2004b.

Du Vivier, A. D. C., Selby, D., Sageman, B. B., Jarvis, I., Gröcke, D. R., and Voigt, S.: Marine ^{187}Os / ^{188}Os isotope stratigraphy reveals the interaction of volcanism and ocean circulation during Oceanic Anoxic Event 2, Earth Planet. Sc. Lett., 389, 23–33, 2014.

Eldrett, J. S., Minisini, D., and Bergman, S. C.: Decoupling of the carbon cycle during Ocean Anoxic Event 2, Geology, 42, 567–570, 2014.

Eldrett, J. S., Ma, C., Bergman, S. C., Lutz, B., Gregory, J., Dodsworth, P., Phipps, M., Hardas, P., Minisini, D., Ozkan, A., Ramezani, J., Bowring, S., Kamo, S., Ferguson, K., MacAulay, C., and Kelly, A.: An astronomically calibrated stratigraphy of the Cenomanian–Turonian Eagle Ford Formation, Texas, USA: implications for global chronostratigraphy, Cretaceous Res., 56, 316–344, 2015.

Erba, E.: Calcareous nannofossils and Mesozoic oceanic anoxic events, Mar. Micropaleontol., 52, 85–106, 2004.

Fauconnier, D. and Masure, E.: Les dinoflagellés fossiles: guide pratique de détermination: les genres à processus et à archéopyle apical. Editions BRGM, Collection Scientifique, Orléans, France, 600 pp., 2004.

Fensome, R. A. and Williams, G. L.: The Lentin and Williams Index of Fossil Dinoflagellates, 2004 Edn., American Association of Stratigraphic Palynologists Contribution Series, Dallas, Texas, USA, 42, 909 pp., 2004.

Forster, A., Schouten, S., Moriya, K., Wilson, P. A., and Sinninghe Damsté, J. S.: Tropical warming and intermittent cooling during the Cenomanian/Turonian oceanic anoxic event 2: sea-surface temperature records from the equatorial Atlantic, Palaeoceanography, 22, PA1219, doi:10.1029/2006PA001349, 2007.

Gale, A. S. and Christensen, W. K.: Occurrence of the belemnite *Actinocamax plenus* in the Cenomanian of SE France and its significance, Bull. Geol. Soc. Den., 43, 68–77, 1996.

Gale, A. S., Kennedy, W. J., Voigt, S., and Walaszczyk, I.: Stratigraphy of the Upper Cenomanian–Lower Turonian Chalk succession at Eastbourne, Sussex, UK: ammonites, inoceramid bivalves and stable carbon isotopes, Cretaceous Res., 26, 460–487, 2005.

Galeotti, S., Brinkhuis, H., and Huber, M.: Records of post–Cretaceous-Tertiary boundary millennial-scale cooling from the western Tethys: A smoking gun for the impact-winter hypothesis?, Geology, 32, 529–532, 2004.

Gradstein, F. M., Ogg, J. G., Schmitz, M. D., and Ogg, G. M.: The Geologic Time Scale 2012, Elsevier, Oxford (UK), 1144 pp., 2012.

Harris, A. J. and Tocher, B. A.: Palaeoenvironmental analysis of Late Cretaceous dinoflagellate cyst assemblages using high-resolution sample correlation from the Western Interior Basin, USA, Mar. Micropaleontol., 48, 127–148, 2003.

Hasegawa, T., Crampton, J. S., Schiøler, P., Field, B., Fukushi, K., and Kakizaki, Y.: Carbon isotope stratigraphy and depositional oxia through Cenomanian/Turonian boundary sequences (Upper Cretaceous) in New Zealand, Cretaceous Res., 40, 61–80, 2013.

Huber, B. T., Norris, R. D., and MacLeod, K. G.: Deep-sea paleotemperature record of extreme warmth during the Cretaceous, Geology, 30, 123–126, 2002.

Jarvis, I., Carson, G. A., Cooper, M. K. E., Hart, M. B., Leary, P. N., Tocher, B. A., Horne, D., and Rosenfeld, A.: Microfossil assemblages and the Cenomanian–Turonian (Late Cretaceous) oceanic anoxic event, Cretaceous Res., 9, 3–103, 1988.

Jarvis, I., Lignum, J. S., Gröcke, D. R., Jenkyns, H. C., and Pearce, M. A.: Black shale deposition, atmospheric CO_2 drawdown, and cooling during the Cenomanian–Turonian Oceanic Anoxic Event, Paleoceanography, 26, PA3201, doi:10.1029/2010PA002081, 2011.

Jefferies, R. P. S.: The stratigraphy of the *Actinocamax plenus* Subzone (Turonian) in the Anglo-Paris Basin, P. Geologist. Assoc., 74, 1–33, 1963.

Jenkyns, H. C.: Geochemistry of oceanic anoxic events, Geochem. Geophy., Geosy., 11, Q03004, doi:10.1029/2009GC002788, 2010.

Kennedy, W. J., Walaszczyk, I., and Cobban, W. A.: Pueblo, Colorado, USA, candidate Global Boundary Stratotype section and

Point for the base of the Turonian Stage of the Cretaceous, and for the base of the Middle Turonian Substage, with a revision of the Inoceramidae (Bivalvia), Acta Geol. Polon., 50, 295–334, 2000.

Kuypers, M. M. M., Pancost, R. D., and Sinninghe Damsté, J. S.: A large and abrupt fall in atmospheric CO_2 concentration during Cretaceous times, Nature, 399, 342–345, 1999.

Lamolda, M. A. and Mao, S.: The Cenomanian–Turonian boundary event and dinocyst record at Ganuza (northern Spain), Palaeo-geogr. Palaeocl., 150, 65–82, 1999.

Li, H. and Habib, D.: Dinoflagellate stratigraphy and its response to sea level change in Cenomanian-Turonian sections of the West-ern Interior of the United States, Palaios, 11, 15–30, 1996.

Lignum, J. S.: Cenomanian (upper Cretaceous) palynology and chemostratigraphy: Dinoflagellate cysts as indicators of palaeoenvironmental and sea-level change, Ph.D thesis, Kingston University London, Kingston upon Thames, UK, 582 pp., 2009.

Marshall, K. L. and Batten, D. J.: Dinoflagellate cyst associations in Cenomanian– Turonian "black shale" sequences of northern Europe, Rev. Palaeobot. Palyno., 54, 85–103, 1988.

Meyers, S. R., Sageman, B. B., and Arthur, M. A.: Obliquity forc-ing and the amplification of high-latitude climate processes dur-ing Oceanic Anoxic Event 2, Paleoceanography, 27, PA3212, doi:10.1029/2012PA002286, 2012.

McMinn, A.: Outline of a Late Cretaceous dinoflagellate zonation of northern Australia, Alcheringa, 12, 137–156, 1988.

Mohr, B. A., Wähnert, V., and Lazarus, D.: Mid-Cretaceous paleob-otany and palynology of the central Kerguelen Plateau, Southern Indian Ocean (ODP leg 183, site 1138), edited by: Frey, F. A., Coffin, M. F., Wallace, P. J., and Quilty, P. G., Proc. ODP: Sci. Results, College Station, Texas, Ocean Drilling Program, 183, 1–39, 2002.

Paul, C. R. C., Lamolda, M. A., Mitchell, S. F., Vaziri, M. R., Goros-tidi, A., and Marshall, J. D: The Cenomanian/Turonian boundary at Eastbourne (Sussex, UK): a proposed European reference sec-tion, Palaeogeogr. Palaeocl., 150, 83–121, 1999.

Pavlishina, P. and Wagreich, M.: Biostratigraphy and paleoenviron-ments in a northwestern Tethyan Cenomanian-Turonian bound-ary section (Austria) based on palynology and calcareous nanno-fossils, Cretaceous Res., 38, 103–112, 2012.

Pearce, M. A., Jarvis, I., and Tocher, B. A.: The Cenomanian-Turonian boundary event, OAE 2 and palaeoenvironmental change in epicontinental seas: new insights from the dinocyst and geochemical records, Palaeogeogr. Palaeocl., 280, 207–234, 2009.

Peyrot, D., Barroso-Barcenilla, F., Barrón, E., and Comas-Rengifo, M. J.: Palaeoenvironmental analysis of Cenomanian–Turonian dinocyst assemblages from the Castilian Platform (northern-Central Spain), Cretaceous Res., 32, 504–526, 2011.

Peyrot, D., Barroso-Barcenilla, F., and Feist-Burkhardt, S.: Palaeoenvironmental controls on late Cenomanian–early Turo-nian dinoflagellate cyst assemblages from Condemios (Central Spain), Rev. Palaeobot. Palyno., 180, 25–40, 2012.

Prauss, M. L.: The Cenomanian/Turonian Boundary Event (CTBE) at Wunstorf, north-west Germany, as reflected by marine paly-nology, Cretaceous Res., 27, 872–886, 2006.

Radmacher, W., Mangerud, G., and Tyszka, J.: Dinoflagellate cyst biostratigraphy of Upper Cretaceous strata from two wells in the Norwegian Sea, Rev. Palaeobot. Palyno., 216, 18–32, 2015.

Schiøler, P. and Crampton, J. S.: Dinoflagellate biostratigraphy of the Arowhanan Stage (upper Cenomanian–lower Turonian) in the East Coast Basin, New Zealand, Cretaceous Res., 48, 205–224, 2014.

Schlanger, S. O. and Jenkyns, H. C.: Cretaceous Oceanic Anoxic Events: causes and consequences, Geol. Mijnbouw, 55, 179–184, 1976.

Scotese, C. R.: Atlas of Earth History, volume 1, PALEOMAP Project, Arlington, Texas, USA, 2001.

Sinninghe Damsté, J. S., Kuypers, M. M. M., Pancost, R. D., and Schouten, S.: The carbon isotopic response of algae, (cyano)bacteria, archaea and higher plants to the late Ceno-manian perturbation of the global carbon cycle: Insights from biomarkers in black shales from the Cape Verde Basin (DSDP Site 367), Org. Geochem., 39, 1703–1718, 2008.

Sinninghe Damsté, J. S., van Bentum, E. C., Reichart, G. J., Pross, J., and Schouten, S.: A CO_2 decrease-driven cooling and increased latitudinal temperature gradient during the mid-Cretaceous Oceanic Anoxic Event 2, Earth Planet. Sc. Lett., 293, 97–103, 2010.

Sluijs, A., Brinkhuis, H., Stickley, C. E., Warnaar, J., Williams, G. L., and Fuller, M.: Dinoflagellate cysts from the Eocene–Oligocene transition in the Southern Ocean: Results from ODP Leg 189, edited by: Exon, N. F., Kennett, J. P., and Malone, M. J., Proc. ODP: Sci Results, College Station, Texas, Ocean Drilling Program, 189, 1–42, 2003.

Sluijs, A., Bowen, G. J., Brinkhuis, H., Lourens, L. J., and Thomas, E.: The Palaeocene-Eocene thermal maximum super greenhouse: Biotic and geochemical signatures, age models and mechanisms of global change, in: Deep time perspectives on climate change: Marrying the signal from computer models and biological prox-ies, edited by: Williams, M., Haywood, A. M., Gregory, F. J., and Schmidt, D. N., Micropalaeontological Society Special Pub-lication 2, Geological Society London, London, UK, 323–349, 2007.

Stockmarr, J.: Tablets with spores used in absolute pollen analysis, Pollen et Spores, 13, 615–621, 1971.

Tocher, B. A. and Jarvis, I.: Dinocyst distributions and stratigraphy of two Cenomanian–Turonian boundary (Upper Cretaceous) sec-tions from the western Anglo-Paris Basin, J. Micropalaeontol., 14, 97–105, 1995.

Tsikos, H., Jenkyns, H. C., Walsworth-Bell, B., Petrizzo, M. R., Forster, A., Kolonic, S., Erba, E., Premoli Silva, I., Baas, M., Wagner, T., and Sinninghe Damsté, J. S.: Carbon-isotope stratig-raphy recorded by the Cenomanian–Turonian Oceanic Anoxic Event: correlation and implications based on three key localities, J. Geol. Soc. London, 161, 711–719, 2004.

van Helmond, N. A. G. M., Sluijs, A., Reichart, G. J., Sinninghe Damsté, J. S., Slomp, C. P., and Brinkhuis, H.: A perturbed hy-drological cycle during Oceanic Anoxic Event 2, Geology, 42, 123–126, 2014a.

van Helmond, N. A. G. M., Ruvalcaba Baroni, I., Sluijs, A., Sin-ninghe Damsté, J. S., and Slomp C. P.: Spatial extent and de-gree of oxygen depletion in the deep proto-North Atlantic basin during Oceanic Anoxic Event 2, Geochem. Geophy. Geosy., 15, 4254–4266, 2014b.

van Helmond, N. A. G. M., Sluijs, A., Sinninghe Damsté, J. S., Reichart, G.-J., Voigt, S., Erbacher, J., Pross, J., and Brinkhuis, H.: Freshwater discharge controlled deposition of Cenomanian-

Turonian black shales on the NW European epicontinental shelf (Wunstorf, North Germany), Clim. Past, 11, 495–508, doi:10.5194/cp-11-495-2015, 2015.

van Hinsbergen, D. J. J., de Groot, L. V., van Schaik, S. J., Spakman, W., Bijl, P. K., Sluijs, A., Langereis, C. G., and Brinkhuis, H.: A Paleolatitude Calculator for Paleoclimate Studies, PloS One, 10, e0126946, doi:10.1371/journal.pone.0126946, 2015.

van Simaeys, S., Brinkhuis, H., Pross, J., Williams, G. L., and Zachos, J. C.: Arctic dinoflagellate migrations mark the strongest Oligocene glaciations, Geology, 33, 709–712, 2005.

Varban, B. L. and Plint, A. G.: Allostratigraphy of the Kaskapau Formation (Cenomanian-Turonian) in Subsurface and Outcrop: NE British Columbia and NW Alberta, Western Canada Foreland Basin, B. Can. Petrol. Geol., 53, 357–389, 2005.

Varban, B. L. and Plint, A. G.: Palaeoenvironments, palaeogeography, and physiography of a large, shallow, muddy ramp: Late Cenomanian-Turonian Kaskapau Formation, Western Canada foreland basin, Sedimentology, 55, 201–233, 2008.

Vellekoop, J., Sluijs, A., Smit, J., Schouten, S., Weijers, J. W. H., Sinninghe Damsté, J. S., and Brinkhuis, H.: Rapid short-term cooling following the Chicxulub impact at the Cretaceous–Paleogene boundary, P. Natl. Acad. Sci. USA, 111, 7537–7541, 2014.

Voigt, S., Gale, A. S., and Voigt, T.: Sea-level change, carbon cycling and palaeoclimate during the Late Cenomanian of northwest Europe; an integrated palaeoenvironmental analysis, Cretaceous Res., 27, 836–858, 2006.

Voigt, S., Erbacher, J., Mutterlose, J., Weiss, W., Westerhold, T., Wiese, F., Wilmsen, M., and Wonik, T.: The Cenomanian–Turonian of the Wunstorf section (north Germany): Global stratigraphic reference section and new orbital time scale for oceanic anoxic event 2, Newsl. Stratigr., 43, 65–89, 2008.